Interferometria Diferencial: caracterizando deformación cortical en Latinoamérica desde el espacio

Dr. Ing. Pablo A. Euillades[1,2]

Mendoza, Argentina

2021

[1] Instituto CEDIAC / FI / UNCuyo
[2] CONICET

Interferometría Diferencial SAR (DInSAR)

Usando pares de imágenes SAR tomadas antes y después de un evento que deforma la superficie terrestre es posible **estimar el desplazamiento ocurrido** entre las fechas de las imágenes.

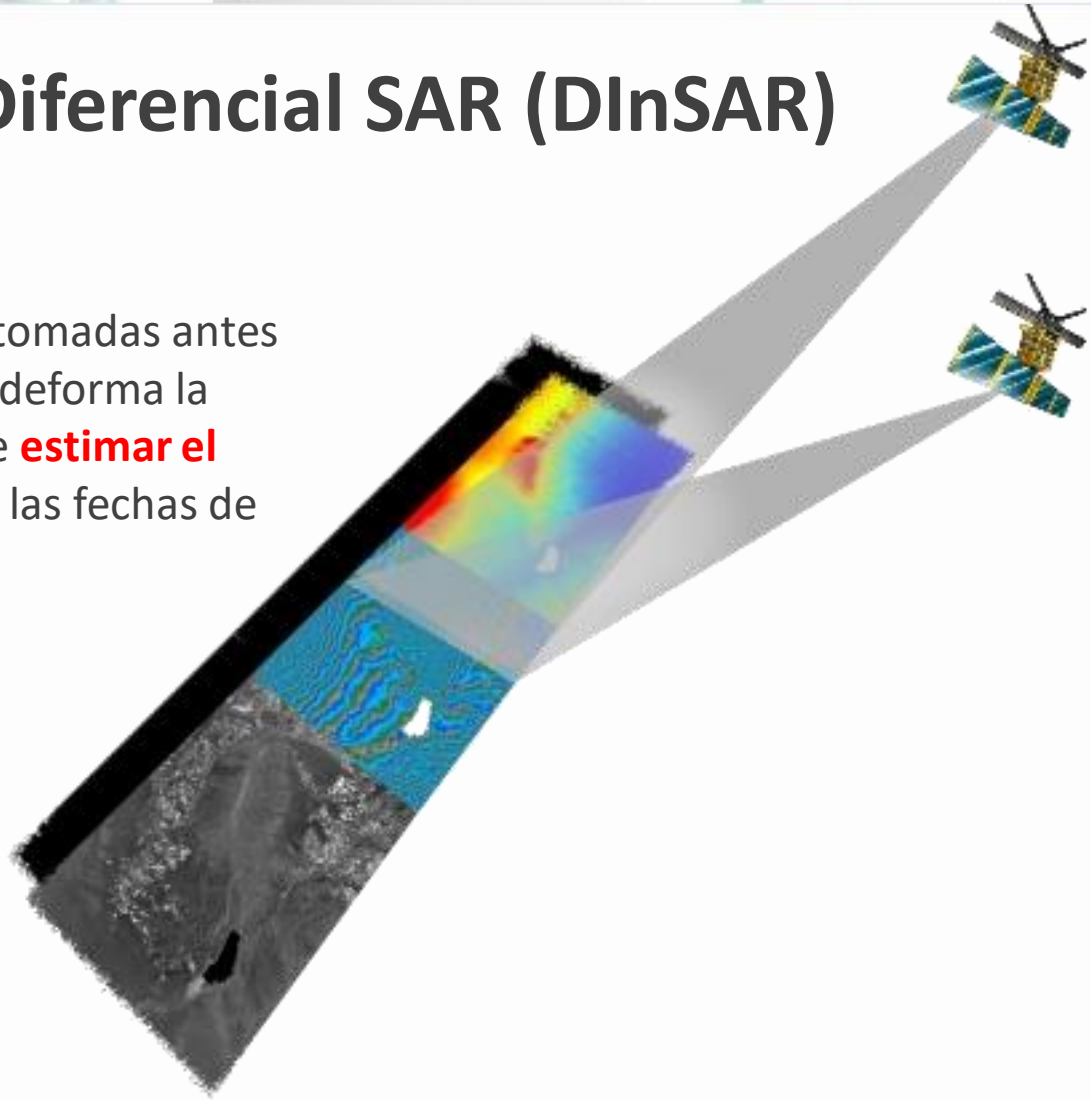

YouTube AR

https://bit.ly/2RvMWqD

Complejo Volcánico Copahue Caviahue (CVCC)

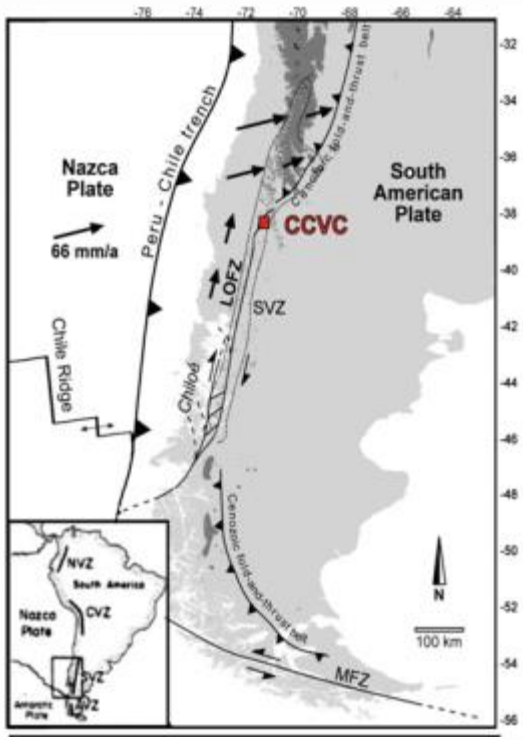

11/11/2011 – 28/10/2012

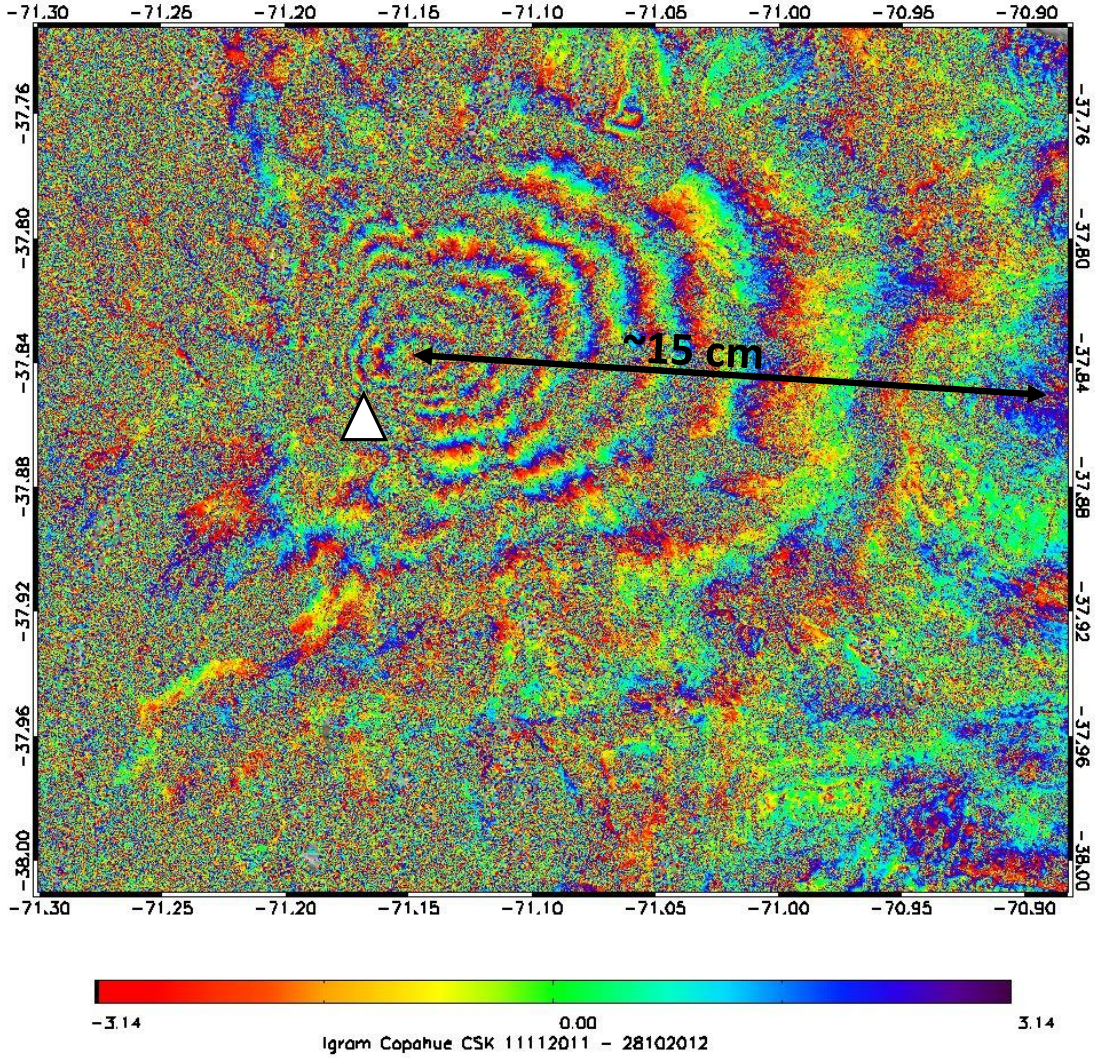

MT-InSAR (SBAS y otras técnicas)

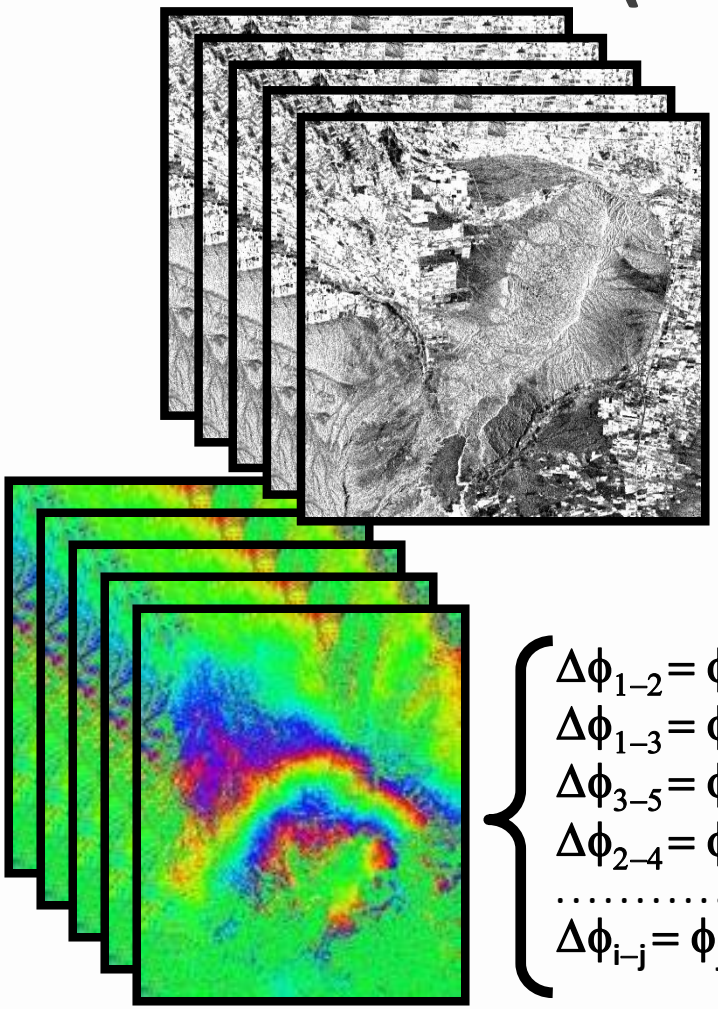

$$\Delta\phi_{1-2} = \phi_2 - \phi_1$$
$$\Delta\phi_{1-3} = \phi_3 - \phi_1$$
$$\Delta\phi_{3-5} = \phi_5 - \phi_3$$
$$\Delta\phi_{2-4} = \phi_4 - \phi_2$$
$$\cdots\cdots\cdots\cdots\cdots$$
$$\Delta\phi_{i-j} = \phi_j - \phi_i$$

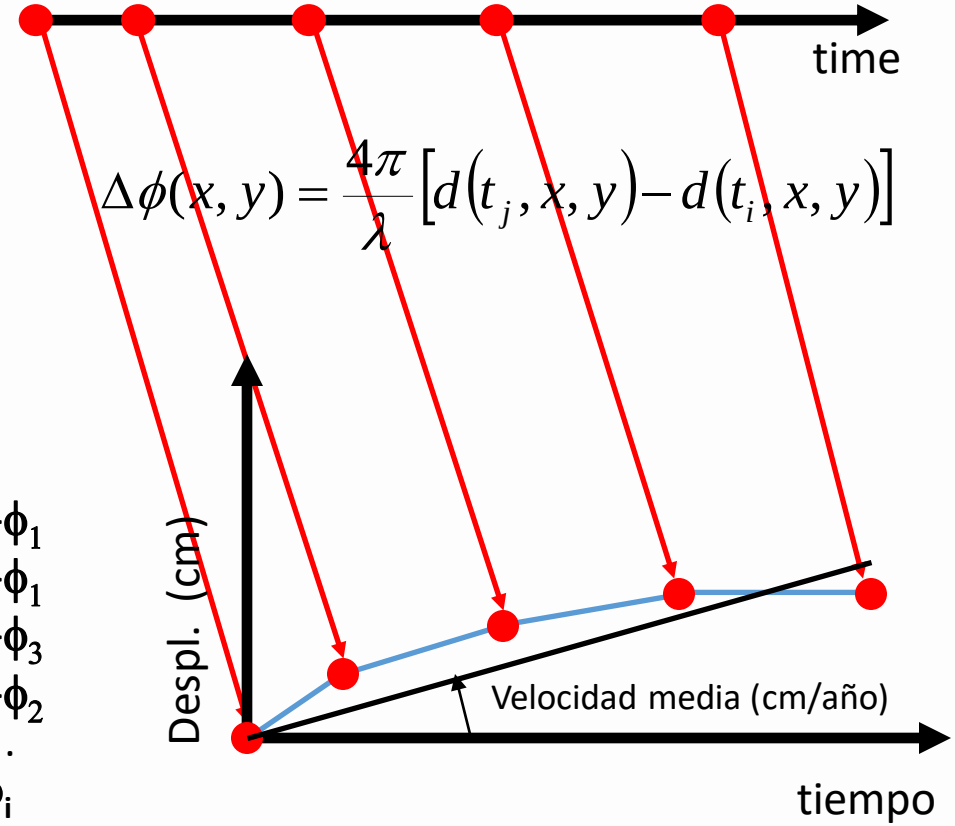

$$\Delta\phi(x,y) = \frac{4\pi}{\lambda}\left[d(t_j,x,y) - d(t_i,x,y)\right]$$

P. Berardino, G. Fornaro, R. Lanari y E. Sansosti, "A new algorithm for surface deformation monitoring based on small baseline differential SAR interferograms", *IEEE TGARS*, Vol. 40, N°11, pp. 2375-2383, 2002.

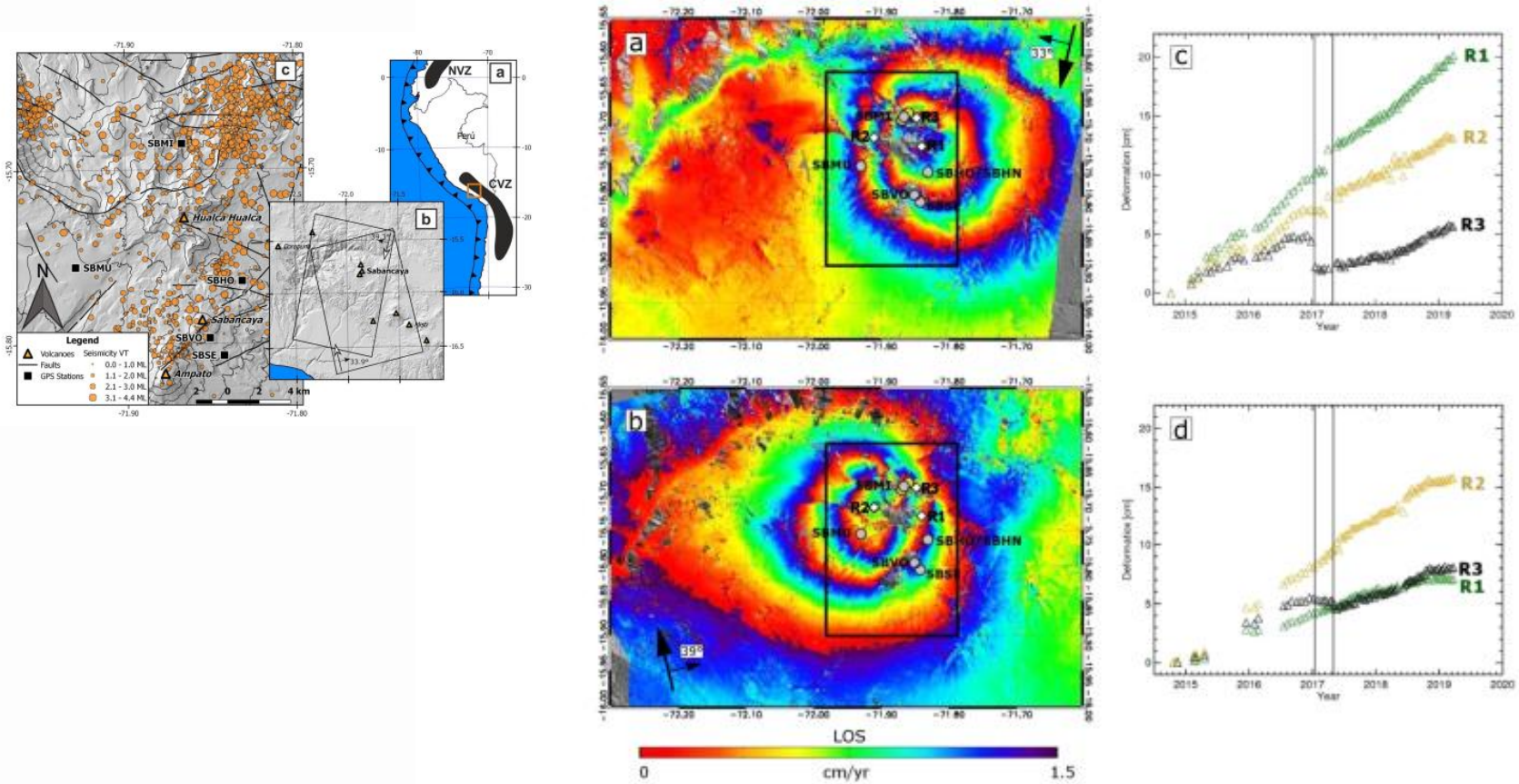

Figure 2. Time series extracted at the positions marked R1, R2, and R3 (white squares) for deformation along the line of sight. Ascending and descending Sentinel-1 orbits (DInSAR) processing results for (**a**) descending and (**b**) ascending orbits. SBMU, SBVO, SBSE, SBMI, and SBHO/SBHN are the locations of the GNSS stations. (**c**) and (**d**) are the deformation time series of the descending and ascending orbits, respectively, extracted from R1, R2, and R3 points. The black vertical lines mark the time of the two 2017 earthquakes. The shape of the deformed area is almost circular, with a diameter of ~45 km, and appears skewed in the opposite direction within Figure 2 because of the SAR lateral view.

Corregistración Geométrica

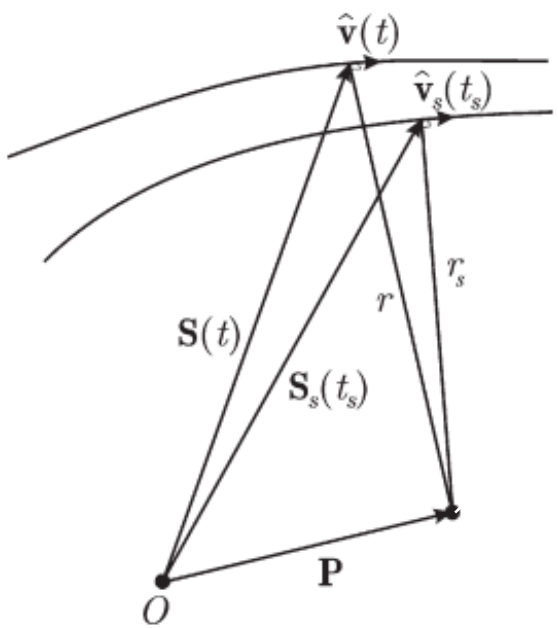

Fig. 1. General geolocation geometry. $\mathbf{P}$ is the vector pointing to the ground point. $\mathbf{S}(t)$ and $\mathbf{S}_s(t_s)$ are the vector functions describing the sensor trajectories. $\hat{\mathbf{v}}(t)$ and $\hat{\mathbf{v}}_s(t_s)$ are the velocity unit vectors, and r and r_s are the ranges for the master and slave acquisitions, respectively.

$$\begin{cases} \tau = \frac{2}{c}\left|\mathbf{P} - \mathbf{S}(t)\right| & \text{Tiempo señal master} \\ \hat{\mathbf{v}}(t) \cdot (\mathbf{P} - \mathbf{S}(t)) = 0 \\ \tau_s = \frac{2}{c}\left|\mathbf{P} - \mathbf{S}_s(t_s)\right| & \text{Tiempo señal slave} \\ \hat{\mathbf{v}}_s(t_s) \cdot (\mathbf{P} - \mathbf{S}_s(t_s)) = 0. \end{cases}$$

$$\mathbf{P} = (P_x, P_y, P_z).$$

Relacionan la posición P con los tiempos en rango (τ) y en azimuth (t) con el nro de pixel i y j a través de:

$$t = t_0 + \frac{1}{\mathrm{PRF}} j$$

$$\tau = \tau_0 + \frac{1}{\mathrm{FS}} i$$

Algoritmo de cálculo de la contribución del terreno

Las posiciones orbitales son especificadas en el sistema cartesiano geocéntrico

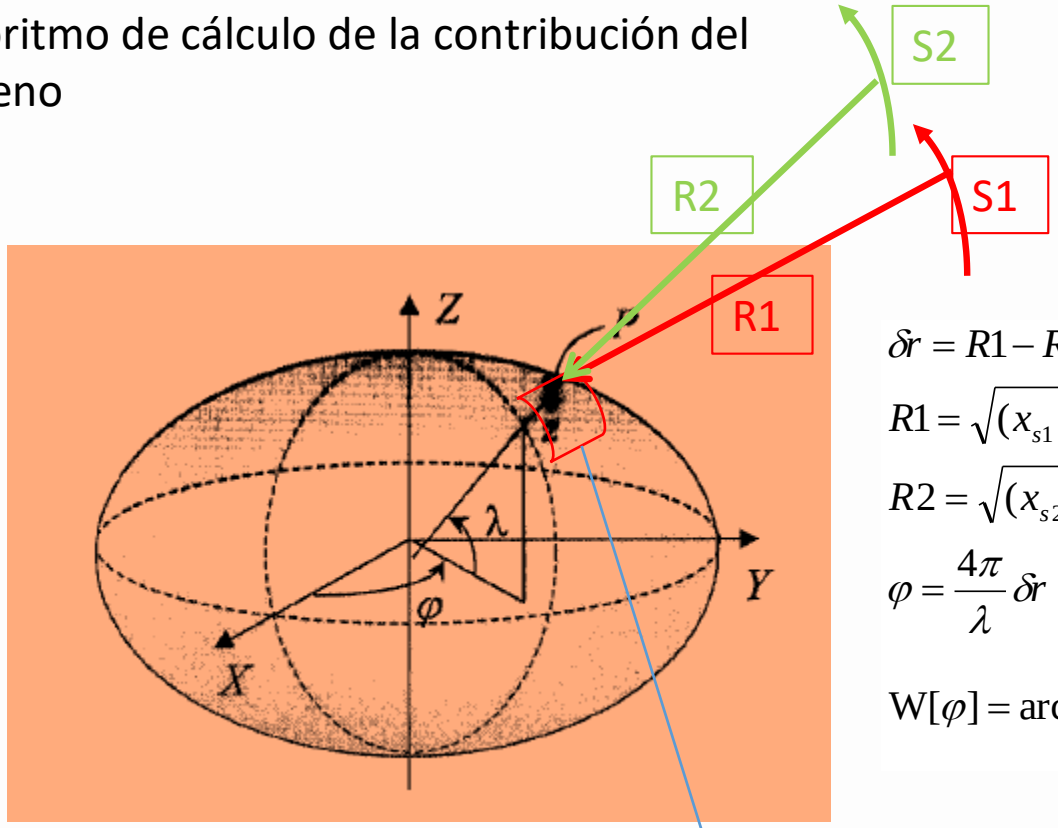

$$\delta r = R1 - R2$$

$$R1 = \sqrt{(x_{s1} - x_P)^2 + (y_{s1} - y_P)^2 + (z_{s1} - z_P)^2}$$

$$R2 = \sqrt{(x_{s2} - x_P)^2 + (y_{s2} - y_P)^2 + (z_{s2} - z_P)^2}$$

$$\varphi = \frac{4\pi}{\lambda}\delta r \quad \text{Contribución de fase de tierra plana}$$

$$\mathrm{W}[\varphi] = \arctan\left[\frac{\sin(\varphi)}{\cos(\varphi)}\right] \quad \text{Interferograma sintético}$$

La imagen es una porción del terreno, y la llamada tierra plana es representada por la superficie del elipsoide de referencia en el sistema cartesiano geocéntrico (XYZ) ¡En realidad no es plana!

Línea de tiempo de los SAR pasados, presentes y futuros

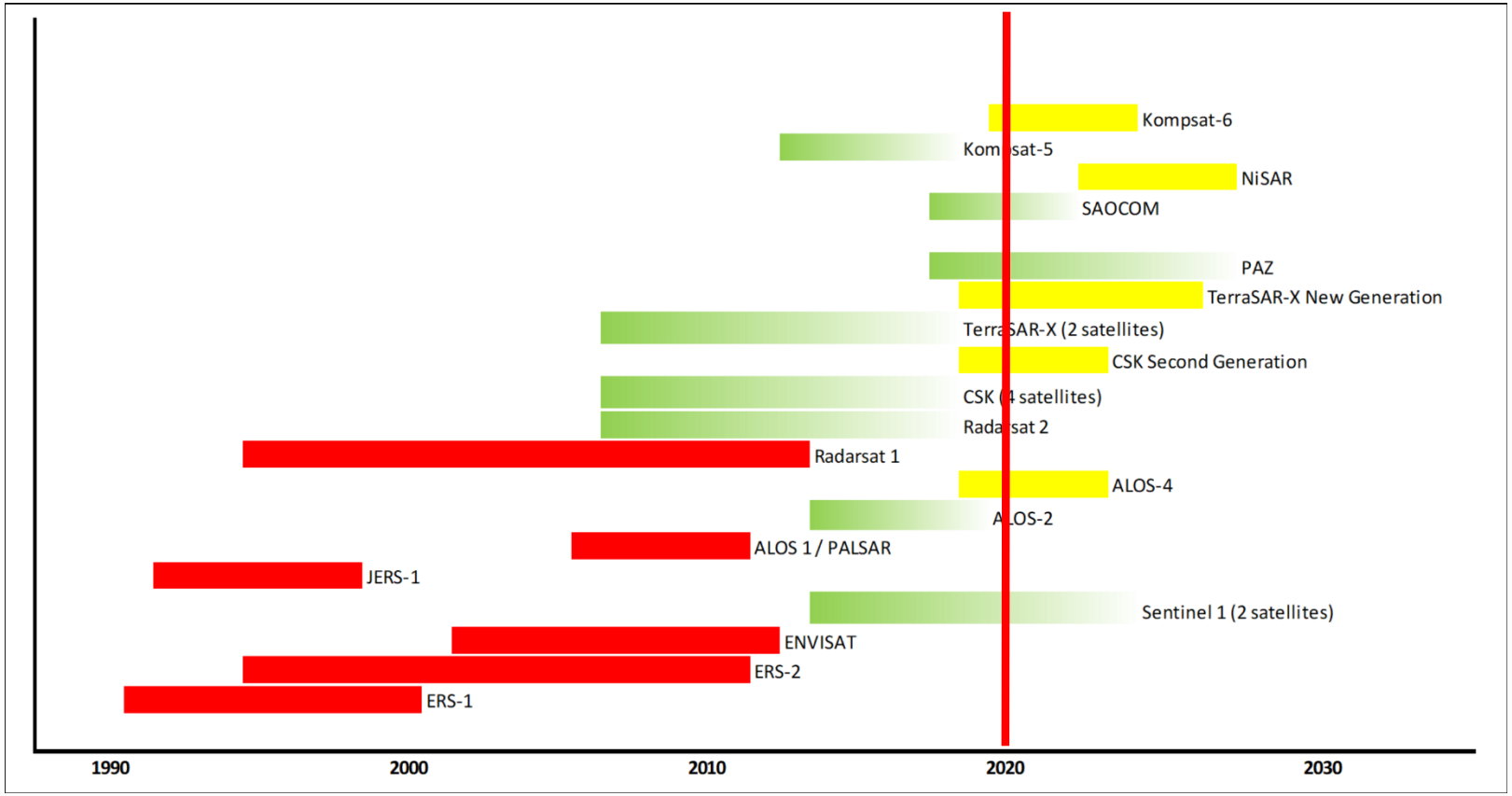

1996 - 2020

- Wetland InSAR
- Remoción en masa
- Glaciares
- Subsidencia Minería
- Vulcanismo
- Terremotos
- Miscelánea

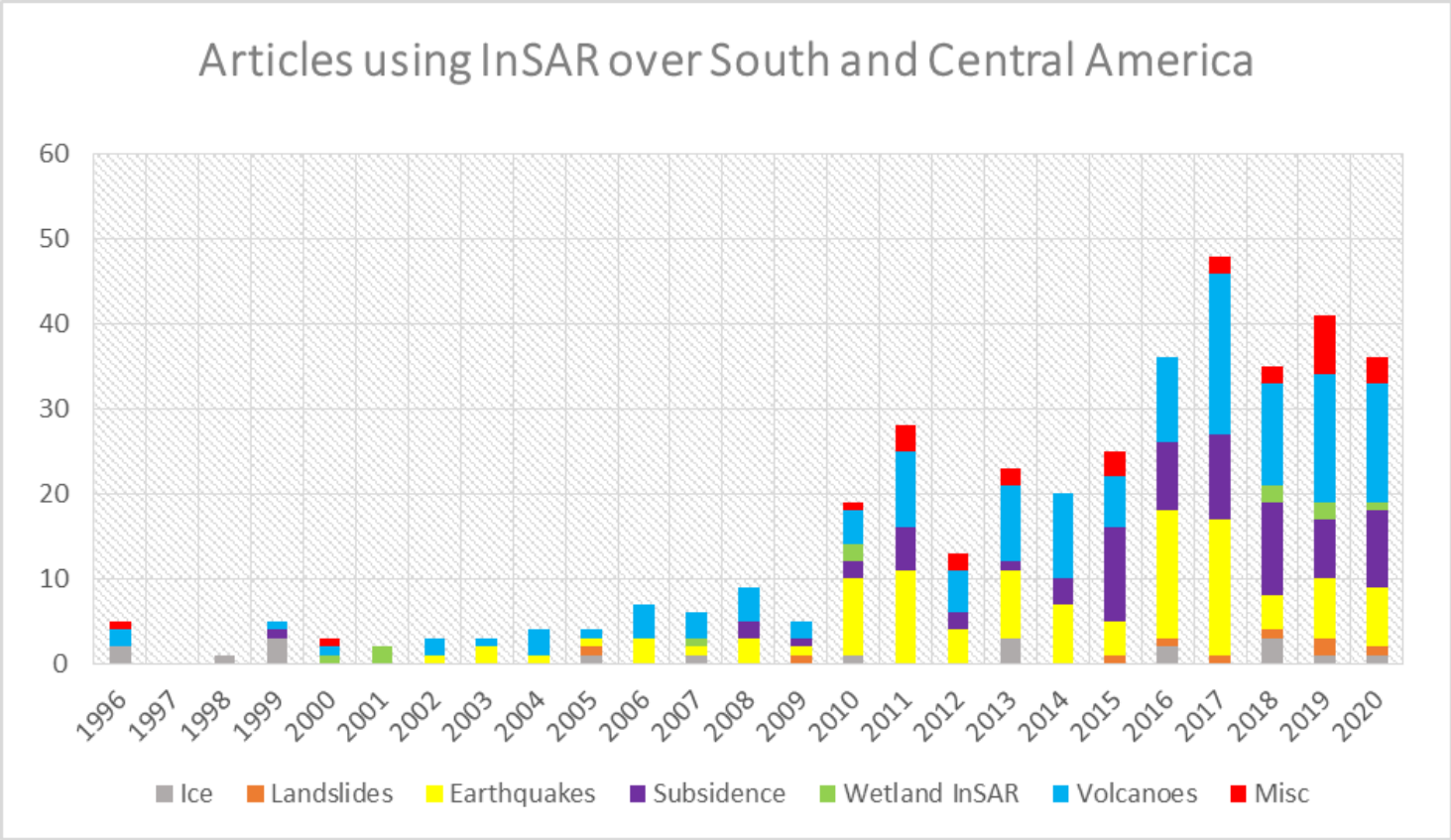
Articles using InSAR over South and Central America
60
50
40
30
20
10
0
1996
1997
1998
1999
2000
2001
2002
2003
2004
2005
2006
2007
2008
2009
2010
2011
2012
2013
2014
2015
2016
2017
2018
2019
2020
Ice
Landslides
Earthquakes
Subsidence
Wetland InSAR
Volcanoes
Misc

Terremotos

~140 Artículos

1998 Mw 8.1 en Antofagasta
2005 Mw 7.7 en Tarapacá, Chile
2007 Mw 8.0 en Pisco, Perú
2010 Mw 7.0 en Haití
2010 Mw 8.8 en Maule,
2014 Mw 8.1 en Iquique, Chile
2015 Mw 8.3 en Illapel, Chile
2016 Mw 7.8 en Pedernales, Ecuador

ELSEVIER

Earth and Planetary Science Letters
Volume 460, 15 February 2017, Pages 222-233

Surface deformation associated with the 2015 M_w 8.3 Illapel earthquake revealed by satellite-based geodetic observations and its implications for the seismic cycle

Wanpeng Feng [a], Sergey Samsonov [a], Yunfeng Tian [b], Qiang Qiu [c], Peng Li [d], Yong Zhang [e], Zhiguo Deng [f], Khalid Omari [a]

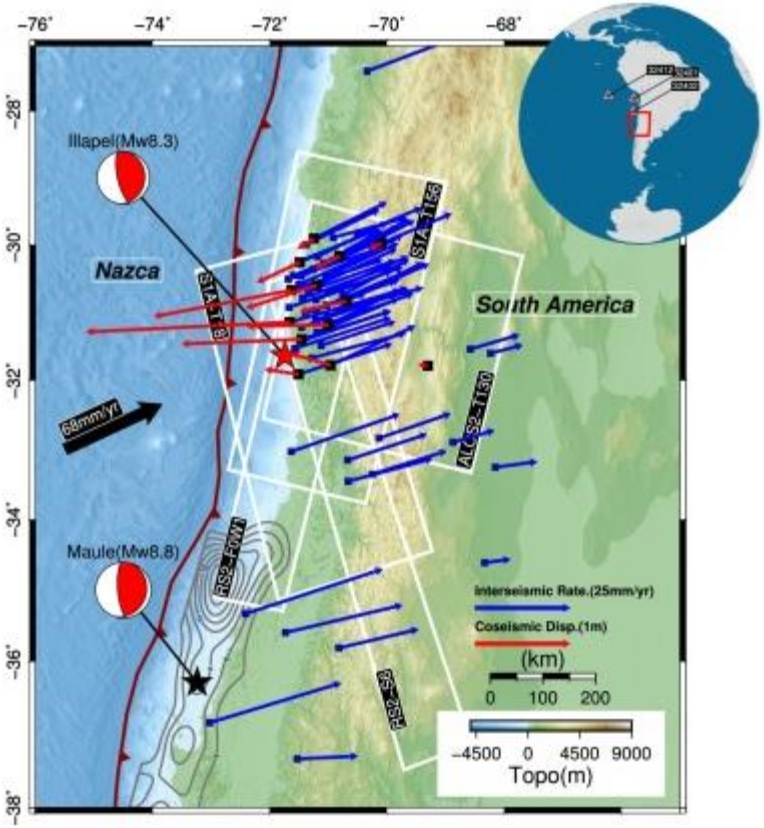

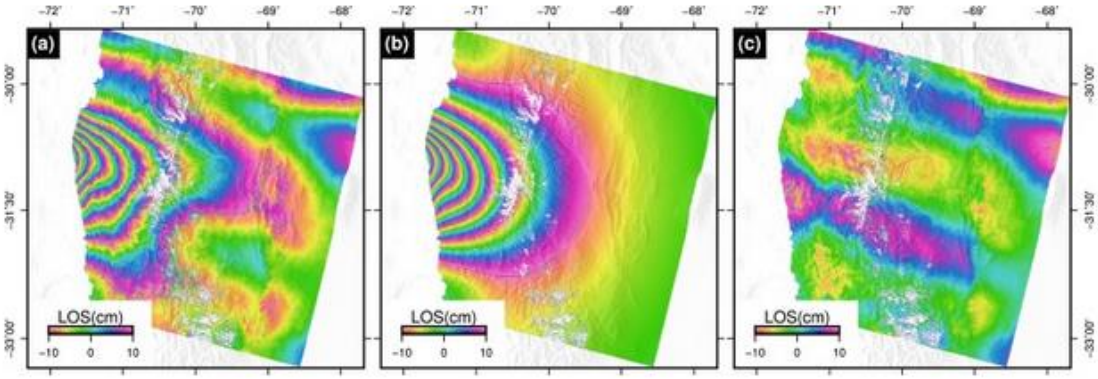

Download : Download high-res image (793KB) Download : Download full-size image

Volcanes

~240 Artículos

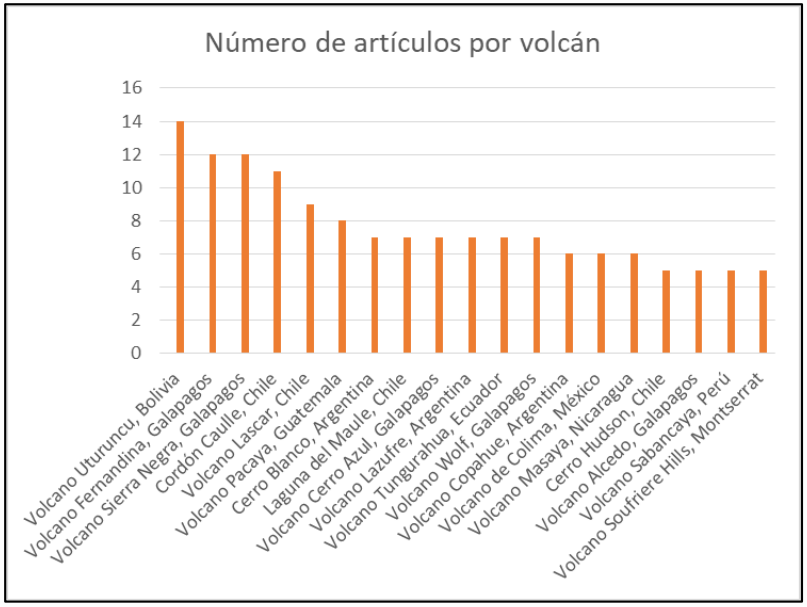

remote sensing

MDPI

Article

Source Model for Sabancaya Volcano Constrained by DInSAR and GNSS Surface Deformation Observation

Gregorio Boixart [1], Luis F. Cruz [2,3], Rafael Miranda Cruz [2], Pablo A. Euillades [4], Leonardo D. Euillades [4] and Maurizio Battaglia [5,6,*]

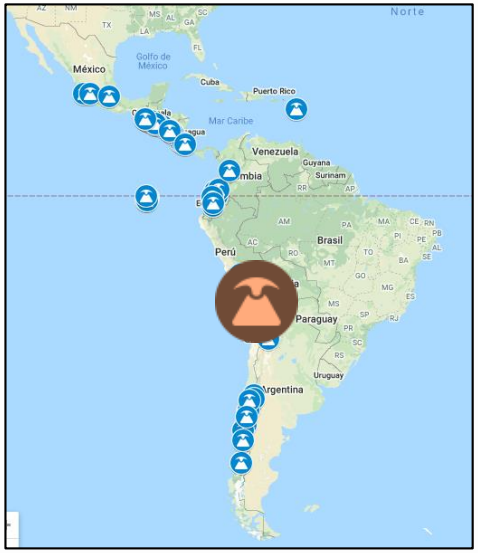

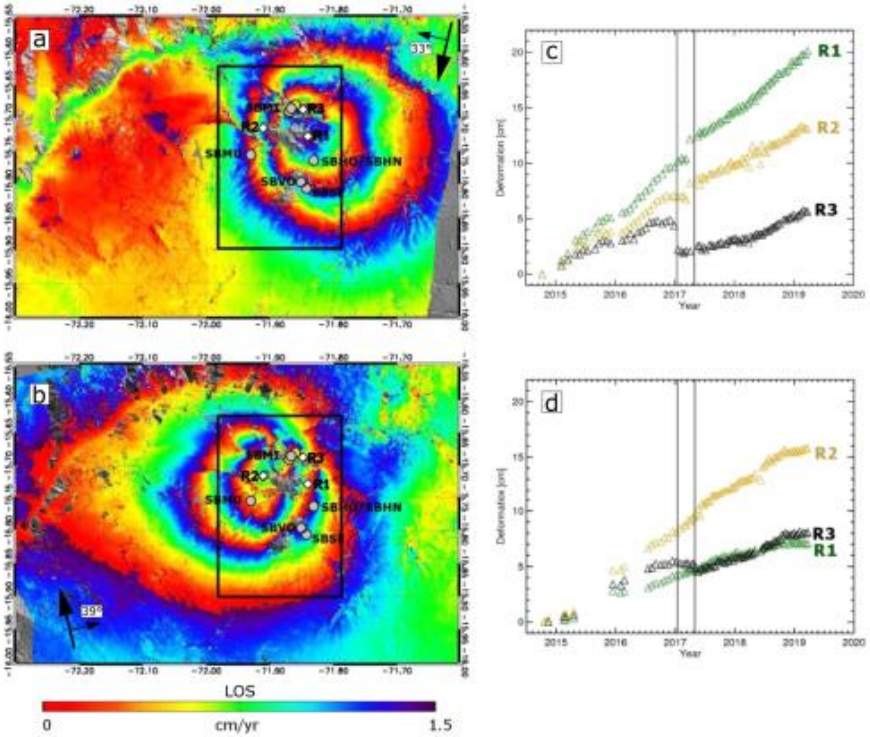

Figure 2. Time series extracted at the positions marked R1, R2, and R3 (white squares) for deformation along the line of sight. Ascending and descending Sentinel-1 orbits (DInSAR) processing results for (**a**) descending and (**b**) ascending orbits. SBMU, SBVO, SBSE, SBMI, and SBHO/SBHN are the locations of the GNSS stations. (**c**) and (**d**) are the deformation time series of the descending and ascending orbits, respectively, extracted from R1, R2, and R3 points. The black vertical lines mark the time of the two 2017 earthquakes. The shape of the deformed area is almost circular, with a diameter of ~45 km, and appears skewed in the opposite direction within Figure 2 because of the SAR lateral view.

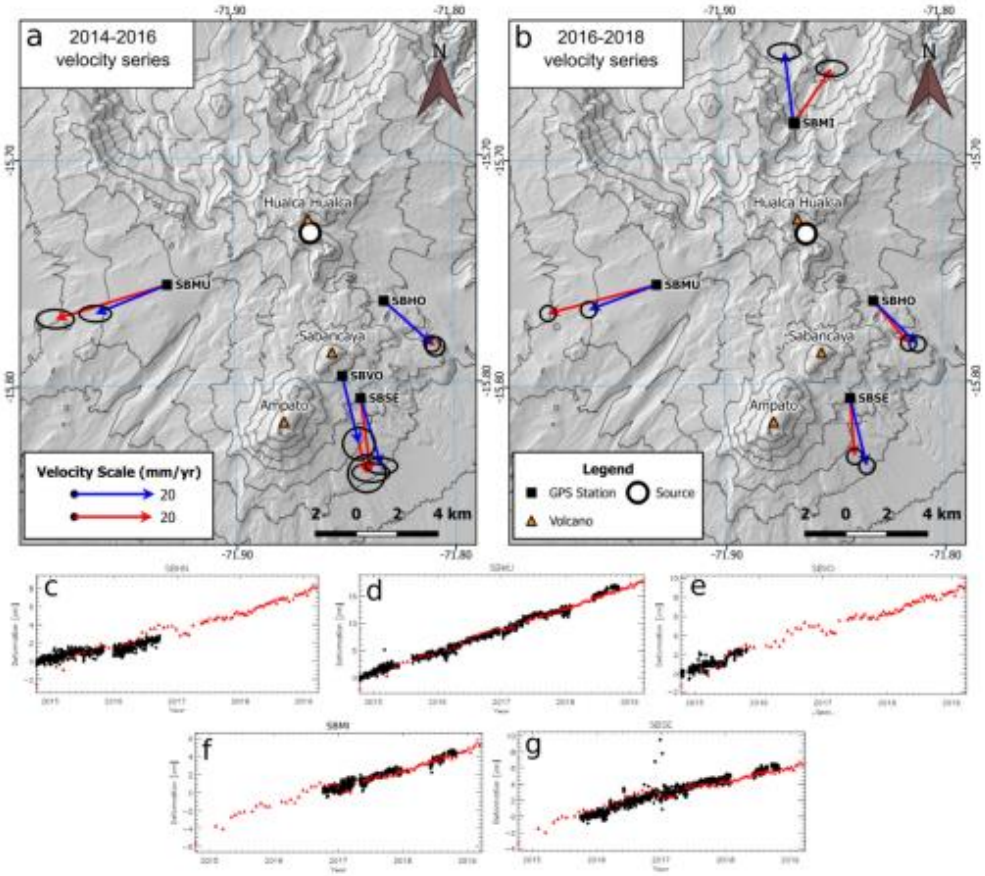

Figure 3. Horizontal velocity vectors produced by the best-fit spherical source (blue) and GNSS data (red) for (**a**) the 2014–2016 velocity series and (**b**) the 2016–2018 velocity series. Note how the data and modelled vectors of the SBMI station differ because of a nearby seismic event. (**c–g**) GNSS deformation series, projected into the ascending Line-of-Sight (LOS), compared to the ascending DInSAR series.

Journal of South American Earth Sciences xxx (xxxx) xxx

Contents lists available at ScienceDirect

Journal of South American Earth Sciences

journal homepage: www.elsevier.com/locate/jsames

ELSEVIER

First assessment of the interferometric capabilities of SAOCOM-1 results over the Domuyo Volcano, Neuquén Argentina

Y. Roa [a,f,*], P. Rosell [a,f], A. Solarte [b,c,f], L. Euillades [a,f], F. Carballo [d], S. García [e], P. I

[a] Instituto CEDIAC, Facultad de Ingeniería, Universidad Nacional de Cuyo, Argentina
[b] Instituto de Altos Estudios Espaciales "Mario Gulich", CONAE-UNC, Argentina
[c] Departamento de Geología Aplicada, Facultad de Ciencias Exactas Físicas y Naturales, Universidad Nacional de Córdoba, Argentina
[d] Servicio Geológico Minero Argentino (SEGEMAR), Argentina
[e] Observatorio Argentino de Vigilancia Volcánica, Servicio Geológico Minero Argentino (SEGEMAR), Argentina
[f] Consejo Nacional de Investigaciones Científicas y Técnicas (CONICET), Argentina

ARTICLE INFO

Keywords:
DinSAR
L-band
SAOCOM
Volcano deformation

ABSTRACT

Differential Interferometric Synthetic Aperture Radar (DInSAR) has
formations with high both spatial and temporal resolutions. The ef
extensively proved using mainly C and X band because of the availabi
frequencies. In vegetated areas, L-band SAR is more adequate becau
decorrelation. This work presents a review of the characteristics of the L
and its potential in deformation monitoring. In order to show it, we
Domuyo Volcano (Neuquén, Argentina). Time series and mean deform
computed using a Sentinel-1 dataset spanning the same time period. Re
between August 2019 and May 2020. As expected and despising the so
mean velocity map is admittedly more coherent in comparison with the S
first time, the computation of deformation time series using SAOCOM

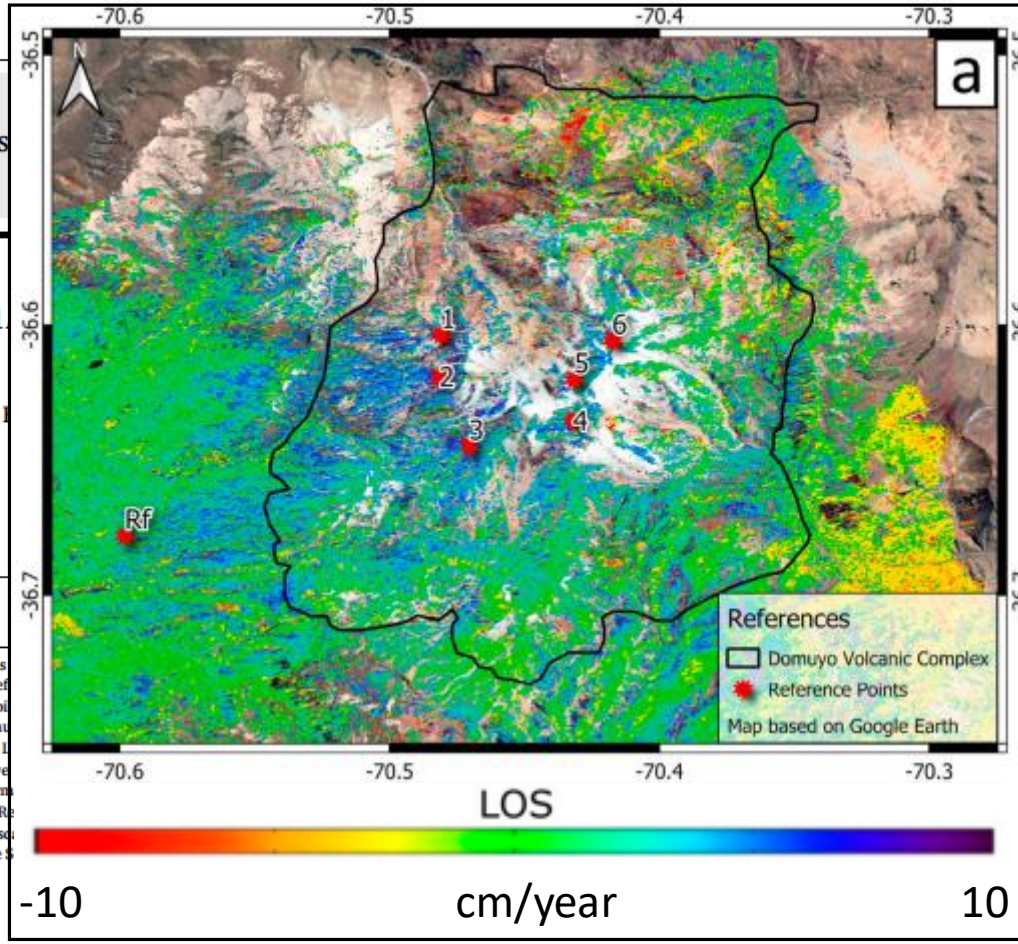

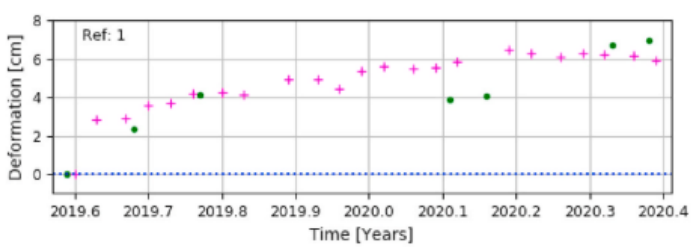

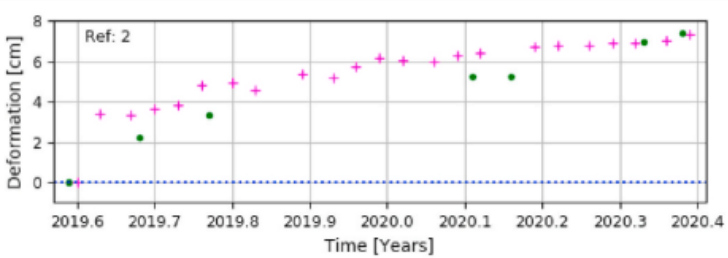

Subsidencia / Minería

~125 Artículos

Explotación de Aguas Subterráneas (México)
Minería (Brasil)

remote sensing

Submit to this Journal

Review for this Journal

Edit a Special Issue

Article Menu

Open Access Article

Deformations Prior to the Brumadinho Dam Collapse Revealed by Sentinel-1 InSAR Data Using SBAS and PSI Techniques

by Fábio F. Gama [1,*], José C. Mura [1], Waldir R. Paradella [1], Cleber G. de Oliveira [2]

Figure 1. (a) Study area location in Minas Gerais state/Brazil; (b) Location of Paraopeba Iron Complex in the Brumadinho municipality; (c) Paraopeba Iron Complex showing tailings Dam I and hydric Dam VI, ancillary mining structures such as ore treatment installation (ITM), rail network, access roads, and a Sentinel-1B descending orbit ground track.

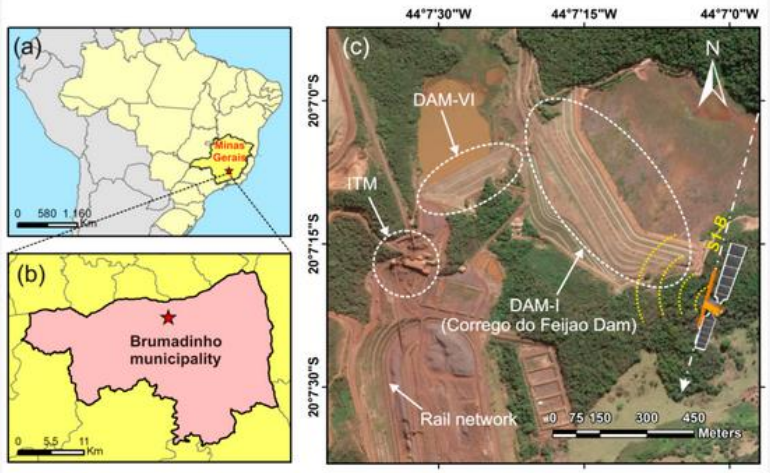

Figure 6. 3D view of Dam-I showing the accumulated displacement from SBAS processing analysis represented by colored dots.

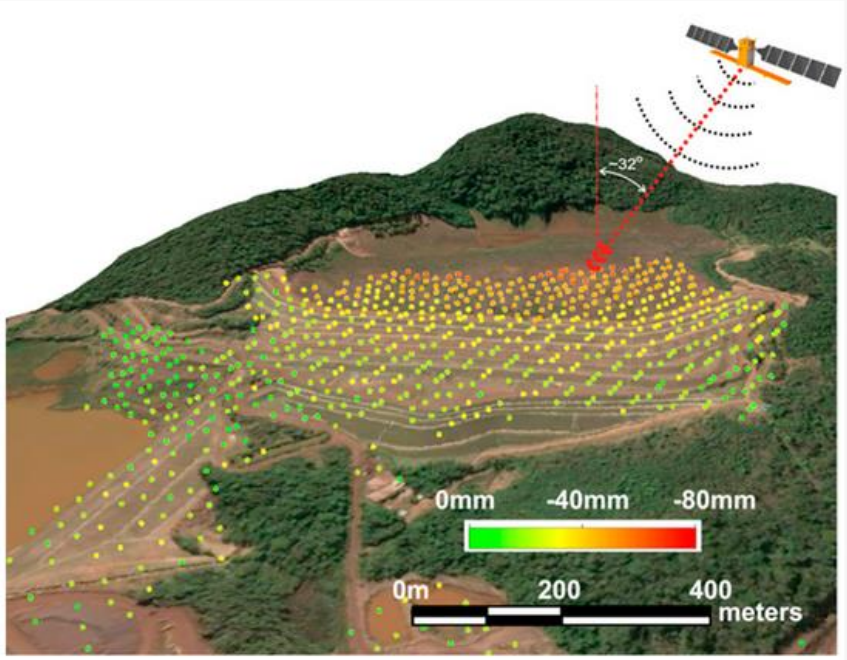

linear regression of the dat

in the text).

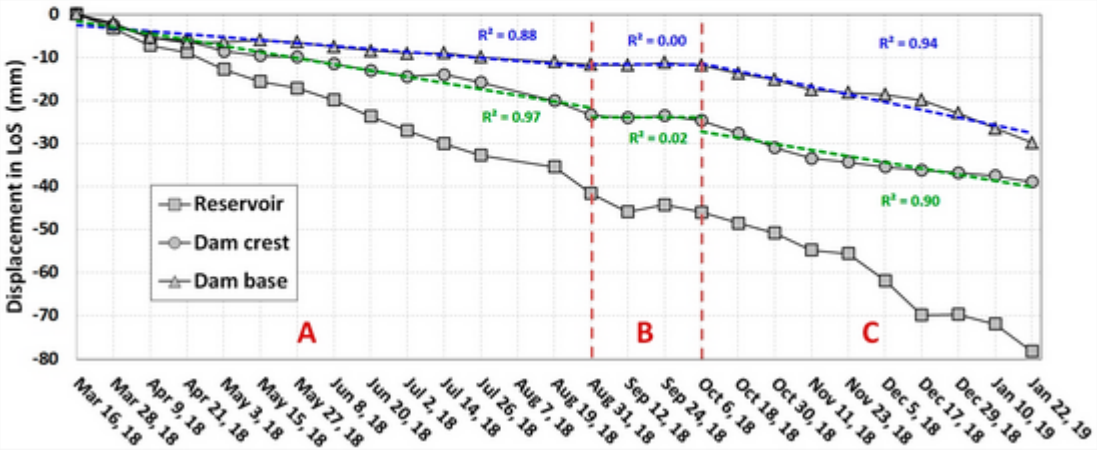

Glaciares

~25 Artículos

Glaciares del Hielo Pat. Sur
Glaciares de escombros

Remote Sensing of Environment 184 (2016) 188–198

Contents lists available at ScienceDirect

Remote Sensing of Environment

journal homepage: www.elsevier.com/locate/rse

Detection of glaciers displacement time-series using SAR

Leonardo D. Euillades [a,b,*], Pablo A. Euillades [a,b], Natalia C. Riveros [a], Mariano H. Masiokas [d], Lucas Ruiz [d], Pierre Pitte [d], Stefano Elefante [c], Francesco Casu [c], Sebastián Balbarani [a,b]

[a] Instituto CEDIAC, Facultad de Ingeniería, Universidad Nacional de Cuyo, cc 405, 5500 Mendoza, Argentina

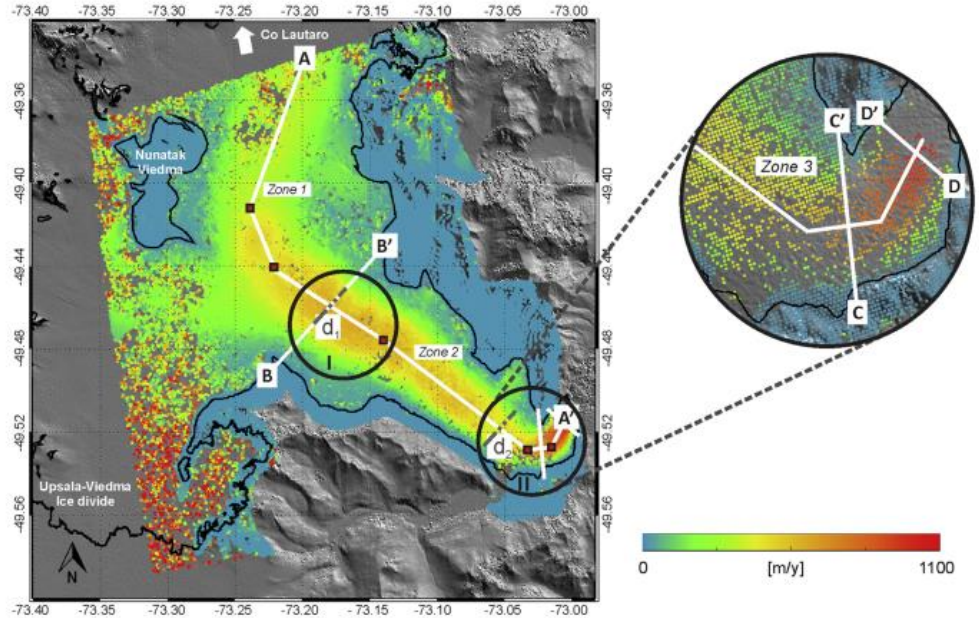

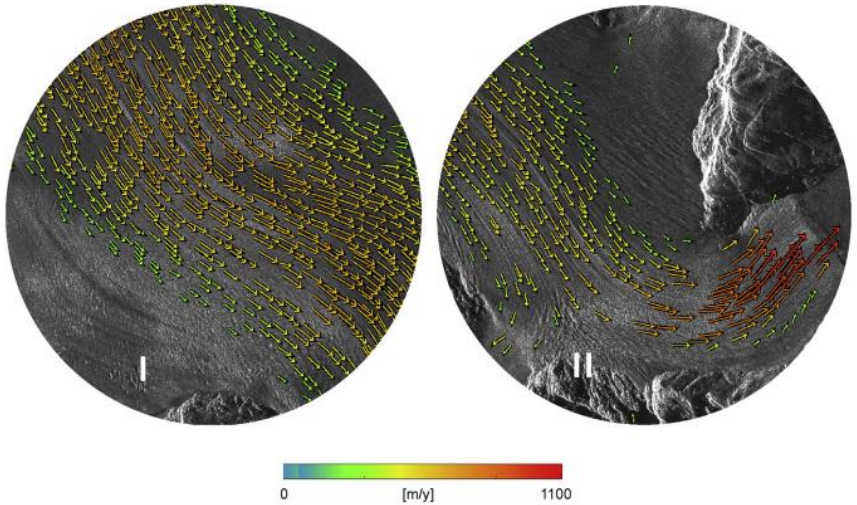

remote sensing

Submit to this Journal

Review for this Journal

Open Access Article

DInSAR for a Regional Inventory of Active Rock Glaciers in the Dry Andes Mountains of Argentina and Chile with Sentinel-1 Data

by Cristian Daniel Villarroel [1,*], Guillermo Tamburini Beliveau [2], Ana Paula Forte [3], Oriol Monserrat [4] and Monica Morvillo [5]

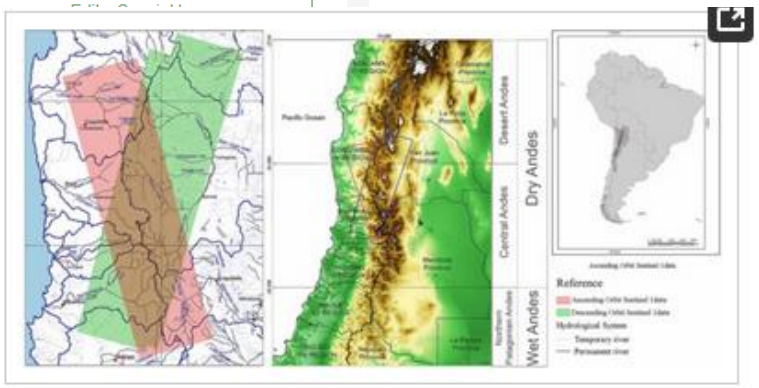

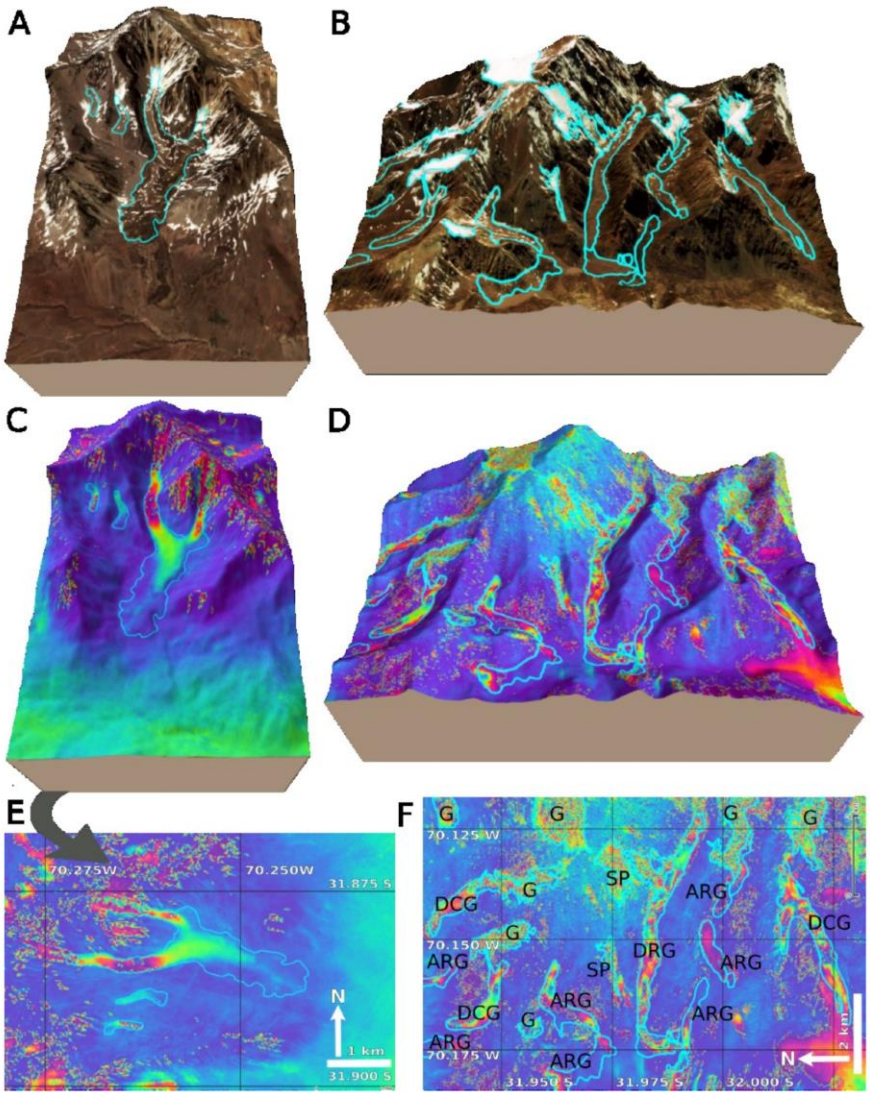

Remoción en masa

~10 Artículos

Original Paper

Landslides
DOI 10.1007/s10346-015-0583-4
Received: 28 June 2014
Accepted: 7 April 2015
© Springer-Verlag Berlin Heidelberg 2015

Clément Michoud · Valérie Baumann · Tom Rune Lauknes · Ivanna Penna · Marc-Henri Derron · Michel Jaboyedoff

Large slope deformations detection and monitoring along shores of the Potrerillos dam reservoir, Argentina, based on a small-baseline InSAR approach

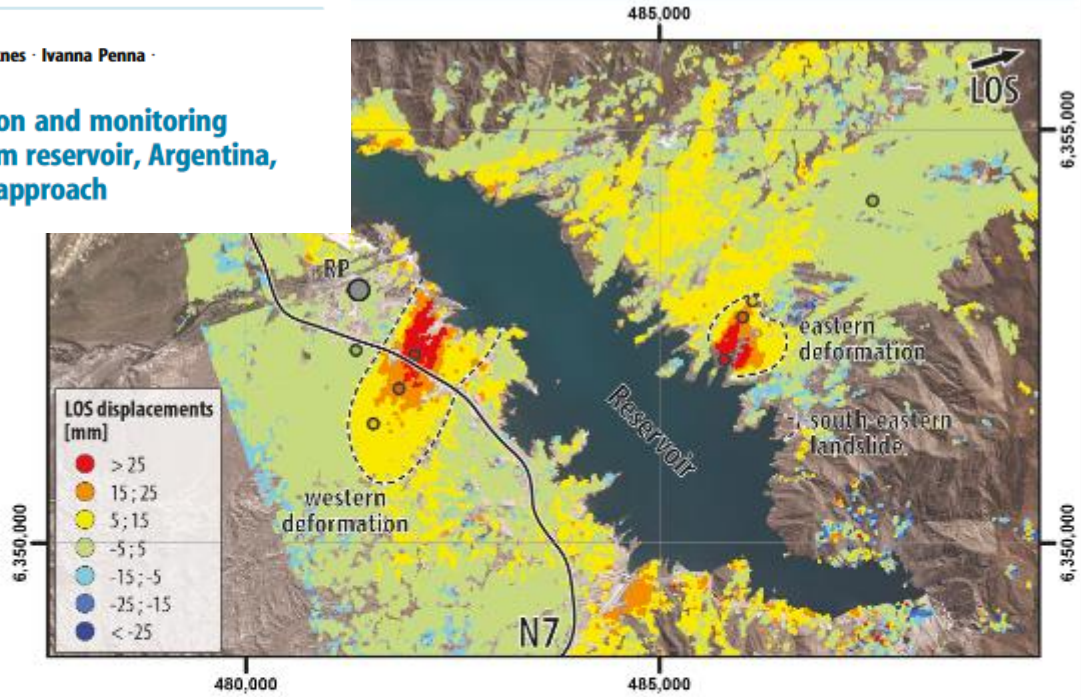

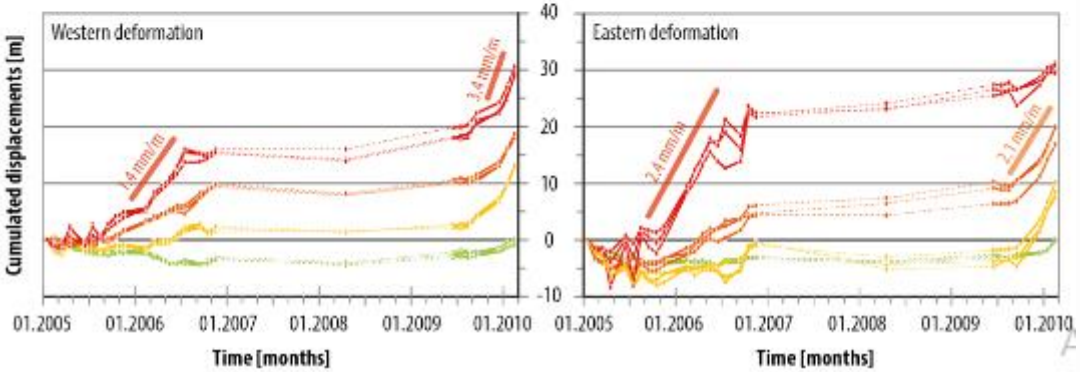

Wetland InSAR

~14 Artículos

Cuenca del Río Amazonas
Detección de cambios

Instituto CEDIAC

water

MDPI

Article

Analysis of Floodplain Dynamics in the Atrato River Colombia Using SAR Interferometry

Sebastián Palomino-Ángel [1,2,*], Jesús A. Anaya-Acevedo [1], Marc Simard [3], Tien-Hao Liao [4] and Fernando Jaramillo [2,5,6]

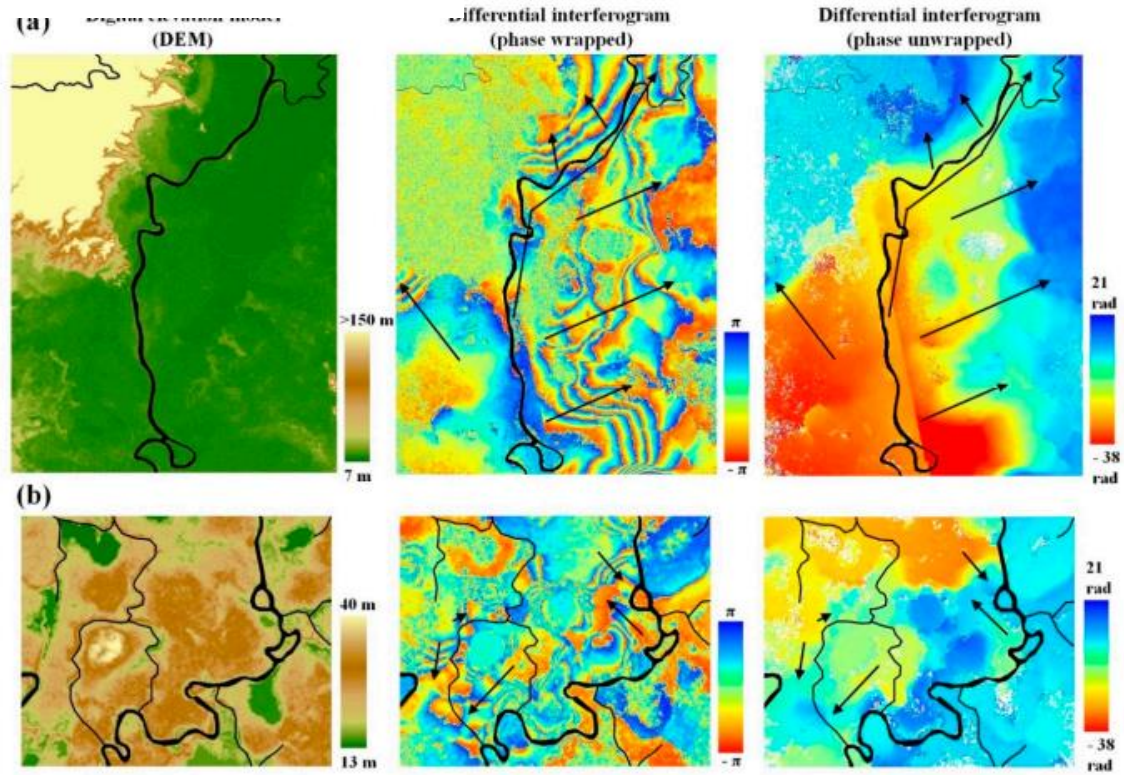

Figure 5. Zooms of Red squares (**a**) Nr. 1 and (**b**) 2 in Figure 3 with the digital elevation model, the wrapped and the unwrapped phase interferograms. The black lines correspond to the main channel of the Atrato River and its tributaries. The arrows indicate the direction of water flow resulting from the DInSAR phase.

Instituto CEDIAC / FI / UNCuyo / ++54 261 4135000 int. 2108 / cc 405 / Mendoza (5500) / Argentina

Instituto CEDIAC
Facultad Ingeniería · UNCuyo
Mendoza · Argentina
5 al 10 de ABRIL 2021

Submit Your Paper
Supports Open Access
View Articles
Guide for Authors
Abstracting/ Indexing
Track Your Paper
Order Journal
Journal Metrics

Call for Paper for Special Issue New advances on SAR Interferometry in South America

"New advances on SAR Interferometry in South America" is a Special Issue aimed to highlight the advances of SAR Interferometry and Speckle Tracking techniques that have been gained in South America since 2014, year in which ESA Sentinel 1's and JAXA ALOS2 sensors began to systematically acquire data over the entire region. Contributions addressing successful application of InSAR based methods in South and Central America, including topics like topographic mapping, crustal deformation, ice motion, atmospheric studies, processing techniques, interferometric coherence studies and other ones InSAR-related, are welcomed.

Feedback

Instituto CEDIAC / FI / UNCuyo / ++54 261 4135000 int. 2108 / cc 405 / Mendoza (5500) / Argentina

ARCHIVO INICIO INSERTAR DISEÑO DE PÁGINA FÓRMULAS DATOS REVISAR VISTA DESARROLLADOR pabloeuillades pabloe

D122 | Deformations Prior to the Brumadinho Dam Collapse Revealed by Sentinel-1 InSAR Data Using SBAS and PSI Techniques

	A	B	C	D	E	F
1	Sensors	Site	Year	Title and link	Authors	Journal
2	ERS	Cerro Prieto, México	1999	Monitoring and modeling land subsidence at the Cerro Prieto Geothermal Field, Baja California, Mexico, using SAR interferometry	Carnec, C., & Fabriol, H.	Geophysical Research Letters
3	ERS, ENVISAT	Ciudad de México, Mexico	2008	Space geodetic imaging of rapid ground subsidence in Mexico City	Cabral-Cano, E., Dixon, T. H., Miralles-Wilhelm, F., Díaz-Molina, O., Sánchez-Zamora, O., & Carande, R. E.	Geological Society of America Bulletin
4	ENVISAT	Morelia, México	2008	DInSAR analysis of differential ground subsidence affecting urban areas along the Mexican Volcanic Belt (MVB)	Farina, P., Avila-Olivera, J. A., Garduño-Monroy, V. H., & Catani, F.	European Journal of Remote Sensing, 103–113.
5		Querétaro, México				
6		Celaya, México				
7	ENVISAT	Ciudad de México, Mexico	2009	Time series analysis of Mexico City subsidence constrained by radar interferometry	López-Quiroz, P., Doin, M.-P., Tupin, F., Briole, P., & Nicolas, J.-M.	Journal of Applied Geophysics
8	ERS, ENVISAT, Radarsat 1	Toluca Valley, Mexico	2010	Land subsidence induced by groundwater pumping, monitored by D-InSAR and field data in the Toluca Valley, Mexico.	Calderhead, A. I., Martel, A., Alasset, P. J., Rivera, A., & Garfias, J.	Canadian Journal of Remote Sensing, 36(1), 9-23.
9	ENVISAT	Cerro Prieto, Baja California, Mexico	2010	Anthropogenic subsidence in the Mexicali Valley, Baja California, Mexico, and slip on the Saltillo fault	Glowacka, E., Sarychikhina, O., Suárez, F., Nava, F. A., & Mellors, R.	Environ Earth Sci, 59:1515–1524
10	ENVISAT	Toluca Valley, Mexico	2011	Simulating pumping-induced regional land subsidence with the use of InSAR and field data in the Toluca Valley, Mexico	Calderhead, A. I., Therrien, R., Rivera, A., Martel, R., & Garfias, J.	Advances in Water Resources, 34(1), 83-97.
11	ENVISAT	Ciudad de México, Mexico	2011	Mexico City subsidence observed with persistent scatterer InSAR	Osmanoğlu, B., Dixon, T. H., Wdowinski, S., Cabral-Cano, E., & Jiang, Y.	International Journal of Applied Earth Observation and Geoinformation
12	ENVISAT	Cerro Prieto, Baja California, Mexico	2011	Land subsidence in the Cerro Prieto Geothermal Field, Baja California, Mexico, from 1994 to 2005: An integrated analysis of DInSAR, leveling and geological data	Sarychikhina, O., Glowacka, E., Mellors, R., Suárez Vidal, F.	Journal of Volcanology and Geothermal Research , 204(1-4) 76-90
13	ERS, ENVISAT	Cerro Prieto, Baja California, Mexico	2011	Aplicación de DInSAR a los estudios de subsidencia en el Valle de Mexicali	Sarychikhina, O., Glowacka, E., Vidal, F. S., Mellors, R., & Hernández, J. R.	Boletín de la Sociedad Geológica Mexicana
14	ENVISAT	Ciudad de México, Mexico	2011	Subsidencia y sus mapas de peligro: Un ejemplo en el área nororiental de la Zona Metropolitana de la Ciudad de México	Cano, E. C., Molina, O. D., & Granados, H. D.	Boletín de la Sociedad Geológica Mexicana
15	ENVISAT	Ciudad de México, Mexico	2012	Mexico City Subsidence Measured by InSAR Time Series: Joint Analysis Using PS and SBAS Approaches	Yan, Y., Doin, M. P., Lopez-Quiroz, P., Tupin, F., Fruneau, B., Pinel, V., & Trouvé, E.	IEEE Journal of Selected Topics in Applied Earth Observations and Remote Sensing, 5(4), 1312-1326.
16	ENVISAT	Morelia, Mexico	2012	Monitoring land subsidence and its induced geological hazard with Synthetic Aperture Radar Interferometry: A case study in Morelia, Mexico	Cigna, F., Osmanoğlu, B., Cabral-Cano, E., Dixon, T. H., Ávila-Olivera, J. A., Garduño-Monroy, V. H., ... Wdowinski, S.	Remote Sensing of the Environment

Ice | Landslides | Earthquakes | **Subsidence-Mining** | Wetland Insar | Volcanoes | Others (Different Topics) ...

¡¡¡ MUCHAS GRACIAS POR SU ATENCIÓN !!!

Información de contacto

pablo.euillades@ingeniería.uncuyo.edu.ar